Structural Properties and Phase Transition of Lithium/Copper Oxides, Depending on $Cu_xLi_{2-x}O$ ($x = 0$, 1, 2) System — *Ab Initio* Study

H. Rekab-Djabri[a,b,*], S. Daoud[c], M.M. Abdus Salam[d] and S. Louhibi-Fasla[a]

[a] *Laboratory of Micro and Nanophysics (LaMiN), National Polytechnic School Oran, ENPO-MA, BP 1523, El M'Naouer, 31000, Oran, Algeria*
[b] *Faculty of Nature and Life Sciences and Earth Sciences, Akli Mohand-Oulhadj University, 10000, Bouira, Algeria*
[c] *Laboratory of Materials and Electronic Systems, Mohamed El Bachir El Ibrahimi University of Bordj Bou Arreridj, Bordj Bou Arreridj, 34000, Algeria*
[d] *Department of Applied Physics, Tafila Technical University, Tafila 66110, Jordan*

Received: 13.01.2021 & Accepted: 19.05.2021

Doi: 10.12693/APhysPolA.140.34 *e-mail: rekabdjabrihamza@yahoo.fr

Structural properties of $Cu_xLi_{2-x}O$ ($x = 0$, 1, 2) system at ambient conditions were presented together with phase transition under high pressure from a cubic cuprite-type (C_3) to an antifluorite-type (C_1) structure of Cu_2O compound ($x = 2$). The calculations were performed using the full potential linear muffin-tin orbitals approach based on the density functional theory. For the exchange-correlation potential term, we applied the local density approximation. For both the C_1 and C_3 phases, the lattice constants versus copper concentration (x) were found to deviate slightly from the linear relationship of Vegard's law. It was found that the phase transition from the C_3 to the C_1 structure for the Cu_2O compound occurs at 82 GPa.

topics: antifluorite (C_1) structure, cuprite (C_3) structure, structural phase transition, FP-LMTO method

1. Introduction

The lithium oxide (Li_2O) material, also called lithia, is one of the main components of high-resistant or conducting glasses (e.g., $Li_2O + B_2O_3$) in which the alkali oxide lowers the melting point of silica [1]. Lithium oxide was also proposed as a material for breeder blankets in deuterium–tritium fusion reactors of the future. It also plays an important role in reducing the work function and thus enhancing the electrical current of photocathodes, and in promoting catalytic reactions and oxidation enhancement of various semiconductor surfaces. Lithium oxide was found to be crystallizing in the cubic antifluorite-type (C_1) structure (space group no. 225) [2]. The details of the antifluorite crystal structure can be found in [3].

Lithium oxide is a key battery material. It is also used in nuclear industry. At low pressures, it normally crystallizes in the antifluorite structure of space group $Fm\bar{3}m$, which contains octahedral voids. Li_2O exhibits super-ionic conductivity at temperatures above 1200 K in which diffusing Li^+ ions carry electrical current by hopping from one void to another. The oxygen atoms, in turn, remain within a rigid framework [4].

Copper oxides exist in a stable form in the bulk phase. They are transition metal compounds, in general, and the high-T superconductors in particular [5]. Recently, copper (Cu)-based nano-ink has been studied extensively for several electronic applications [6, 7]. The stability of copper nanoparticle in air appears robust because the surface of metal copper oxidized into Cu_2O, and the compositions of the oxides vary with exposure time. Kunc et al. [1] have investigated the structural phase transition in Li_2O, from the antifluorite to the anticotunnite structure, using the angle-dispersive synchrotron X-ray powder diffraction. The studies were supported by *ab initio* calculations. Another very recent study was carried out by Yadav et al. [8] on physical properties of the Cu_2O material, especially the structural parameters, electronic band-structure and magnetic properties.

Based on these previous studies, we are interested in the structural parameters and the phase transition of ternary alloys constructed from these two binary compounds (Li_2O and Cu_2O).

TABLE I

Plane wave number NPLW, muffin-tin radius RMT [a.u.], $\boldsymbol{k}$-point mesh and the energy cut-off $E_{\rm cut}$ [Ry] used in our calculation.

Parameters	The antifluorite (C_1) structure			The cuprite (C_3) structure		
	Cu_2O	LiCuO	Li_2O	Cu_2O	LiCuO	Li_2O
total NPLW	5064	5064	5064	38910	38910	38910
RMTS (O)	2.099	1.72	1.844	1.537	1.526	1.707
RMTS (Cu)	2.099	2.189		1.771	1.721	
RMTS (Li)		2.189	1.807		1.721	1.491
$\boldsymbol{k}$-point	(22; 22; 22)	(22; 22; 22)	(22; 22; 22)	(78; 78; 78)	(78; 78; 78)	(78; 78; 78)
$E_{\rm cut}$	163	139	121	223	194	229

Therefore, we have investigated the structural parameters and the phase transition under high pressure of $Cu_xLi_{2-x}O$ (hereafter, $0 \leq x \leq 2$ denotes the molar fraction of Cu). We performed *ab initio* calculations based on the full-potential linear muffin-tin orbital (FP-LMTO) within the density functional theory (DFT). This paper is organized as follows: A brief description of the computational details and methodology is given in Sect. 2. The theoretical results and discussion concerning the structural parameters and the phase transition are given in Sect. 3. Finally, we conclude in Sect. 4.

2. Computational details

In this study, the first-principles calculations are applied using the FP-LMTO-PLW method [9] augmented by a plane wave basis (PLW) based on the DFT [10, 11] — as implemented in the Lmtart code (Mindlab) [12, 13]. The exchange and correlation potential calculation include the local density approximation (LDA) as parameterized by Perdew and Wang [14]. The charge density and the potential are represented inside the muffin-tin spheres (MTS) by spherical harmonics up to $l_{\rm max} = 6$. The integration of $\boldsymbol{k}$ above the Brillouin zone was taken a $22 \times 22 \times 22$ and $78 \times 78 \times 78$ grids according to the tetrahedron method for the C_1 and C_3 structures, respectively. Self-consistent calculations are considered to be converged when the total energy of the system is stable within 10^{-5} Ry. In order to avoid the overlap of atomic spheres, the muffin-tin spheres radius for each atomic position is taken to be different for each case. The muffin-tin radius values (RMTS), the number of plane waves (NPW) and the total cut-off energies used in our calculation are summarized in Table I. The calculations for $Cu_xLi_{2-x}O$ ($0 \leq x \leq 2$) were obtained for two structures: for the antifluorite (C_1) as well as for the cuprite (C_3) phases.

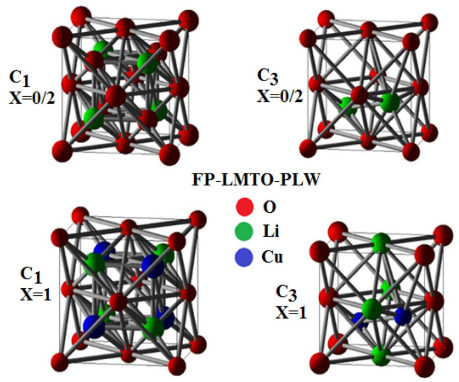

Fig. 1. Cubic crystals of $Cu_xLi_{2x}O$ ($x = 0,\ 1,\ 2$) system in both C_1 and C_3 structures.

The cubic antifluorite C_1 structure (point group: O_h^5; space group: $Fm\bar{3}m$ [#225]), comprises a face-centered cubic sublattice of anions (O^{2-}) with cations (Cu^{2+}, Li^{2+}) on the tetrahedral sites, as shown in Fig. 1.

The cuprite C_3 phase has a high symmetry structure (point group: O_h^4; space group: $Pn\bar{3}m$ [#224]) which is a simple cubic unit cell with two molecules in it. This means only that C_3 has six atoms per unit cell: the two oxygen atoms form a bcc lattice, i.e., one at the corner and another at the body center, while the metal atoms (Cu, Li) are on the vertices of a tetrahedron around each oxygen atom (see Fig. 1).

Each copper atom is two-coordinate with two oxygen atoms. Since both phases have a cubic symmetry, they have only one structural parameter (the lattice constant a) which is used to describe the unit cell.

The positions of different atoms into the unit cell as well as the space group for each of the considered structures of the $Cu_xLi_{2-x}O$ ($x = 0,\ 1,\ 2$) system are summarized in Table II.

3. Results and discussion

3.1. Equation of state parameters

The structural parameters in the ground state were determined by calculating the total energy at different volumes around the equilibrium state for the binary compounds: Li_2O and Cu_2O and their alloy CuLiO. For all the cases, the C_1 and C_3 structures were considered. Next, the calculated total

TABLE II

Location of different atoms and the space group of the C_1 and C_3 structures of the $Cu_xLi_{2-x}O$ (x = 0, 1, 2) system.

Structure type	The antifluorite (C_1) structure			The cuprite (C_3) structure		
Space group	$Fm\bar{3}m$ [#225]			$Pn\bar{3}m$ [#224]		
	$x=0$	$x=1$	$x=2$	$x=0$	$x=1$	$x=2$
1st atom	$(0,0,0)$/Li	$(0,0,0)$/Cu	$(0,0,0)$/Cu	$(0,0,0)$/Li	$(0,0,0)$/Cu	$(0,0,0)$/Cu
2nd atom	$(\frac{1}{4},\frac{1}{4},\frac{1}{4})$/Li	$(\frac{1}{4},\frac{1}{4},\frac{1}{4})$/Li	$(\frac{1}{4},\frac{1}{4},\frac{1}{4})$/Cu	$(0,\frac{1}{2},\frac{1}{2})$/Li	$(0,\frac{1}{2},\frac{1}{2})$/Cu	$(0,\frac{1}{2},\frac{1}{2})$/Cu
3rd atom	$(-\frac{1}{4},-\frac{1}{4},-\frac{1}{4})$/O	$(-\frac{1}{4},-\frac{1}{4},-\frac{1}{4})$/O	$(-\frac{1}{4},-\frac{1}{4},-\frac{1}{4})$/O	$(\frac{1}{2},0,\frac{1}{2})$/Li	$(\frac{1}{2},0,\frac{1}{2})$/Li	$(\frac{1}{2},0,\frac{1}{2})$/Cu
4th atom				$(\frac{1}{2},\frac{1}{2},0)$/Li	$(\frac{1}{2},\frac{1}{2},0)$/Li	$(\frac{1}{2},\frac{1}{2},0)$/Cu
5th atom				$(\frac{1}{4},\frac{1}{4},\frac{1}{4})$/O	$(\frac{1}{4},\frac{1}{4},\frac{1}{4})$/O	$(\frac{1}{4},\frac{1}{4},\frac{1}{4})$/O
6th atom				$(\frac{3}{4},\frac{3}{4},\frac{3}{4})$/O	$(\frac{3}{4},\frac{3}{4},\frac{3}{4})$/O	$(\frac{3}{4},\frac{3}{4},\frac{3}{4})$/O

TABLE III

Structural parameters (equilibrium lattice constants a_0), bulk modulus B_0 and pressure derivatives of the bulk modulus $B_0^{'}$ for the C_1 and C_3 phases for the $Cu_xLi_{2-x}O$ (x = 0, 1, 2) system.

Phase type	x	a [Å]			V [Å^3]	B [GPa]			B_0'			$E_{\min}$ [eV]
			Exp.	Theor.			Exp.	Theor.		Exp.	Theor.	
The antifluorite (C_1)	0	5.130	4.619[a]	4.61[d]	33.76	156.89	81.76[b]	103[d]		3.64	−91926.67	
			4.606[b]	4.573[e]				92.6[e]				
			4.6114[c]	4.573[f]				94.6[f]				
	1	4.776			27.24	106.55			3.64			−47183.18
	2	4.417			21.55	88.76			3.40			−91926.67
The cuprite (C_3)	0	4.374			83.71	188.56			2.88			−91926.38
	1	4.293			79.134	138.06			3.20			−47182.72
	2	4.228	4.2696[g]	4.30[h]	75.59	91.92	112[j]	108[h]	2.83	4.5[k]	4.6–4.8[l]	−2440.36
				4.28[i]			110–112[k]	93[i]				
								104–137[l]				

[a]Ref. [2], [b]Ref. [19], [c]Ref. [20], [d]Ref. [24], [e]Ref. [25], [f]Ref. [26], [g]Ref. [21], [h]Ref. [27], [i]Ref. [28], [j]Ref. [22], [k]Ref. [23], [l]Ref. [29].

energy values were fitted to the Murnaghan equation of state (EOS) [15–18] and the results were plotted in Fig. 2. Now, one can clearly see that at ambient conditions, the antifluorite-type C_1 structure has lower energy than the cuprite-type C_3 for $x = 0$ and $x = 1$ concentrations (i.e., lower by 1.96 eV for $x = 0$ and 0.462 eV for $x = 1$). It means that for the considered concentration, the C_1 structure is more stable than C_3. Further, C_3 is more stable for concentration $x = 2$ since it has lower energy than the C_1 structure (by ≈ 1.66 eV).

The calculated structural parameters, such as the equilibrium lattice constant a_0, the bulk modulus B_0 and the bulk modulus pressure derivative B', for C_1 and C_3 structures, are listed in Table III. Some of the available experimental [2, 19–23] and other theoretical results [24–29] are also included.

Our results for lattice constants a for the C_1 and C_3 structures of the binary compounds (Cu_2O and Li_2O) and the ternary alloy (CuLiO) are listed in Table III. Only the results of the lattice constant of Li_2O in the C_1 phase appear to be higher than the experimental results [2, 19, 20]. In general, however, our results of Cu_2O in the C_3 phase agreed well with other values known from the literature. The lattice constant (4.228 Å) of Cu_2O in the C_3 phase is only 0.97% less than the experimental result (4.2696 Å) [21]. It is also noticeable that our result for the lattice constant of Cu_2O in the C_3 phase is slightly lower than theoretical results (4.30) and (4.28) reported in [27] and [28], respectively.

Our result (91.92 GPa) regarding B_0 for the C_3 phase of the Cu_2O binary material is in reasonable agreement with the result (93 GPa) of [28]. The difference does not exceed the value of 1.2%. To the best of our knowledge, there are no data available in the literature for the C_1 structure of this material.

Usually, in the treatment of alloys, such as LiCuO, when the experimental data are scarce, it is assumed that the atoms are located at the ideal lattice sites. Then, the lattice constant varies linearly with composition x according to the so-called Vegard law [30]:

$$a\big(\mathrm{A}_x\mathrm{B}_{1-x}\mathrm{C}\big) = x a_{\mathrm{AC}} + (1-x)a_{\mathrm{BC}}, \qquad (1)$$

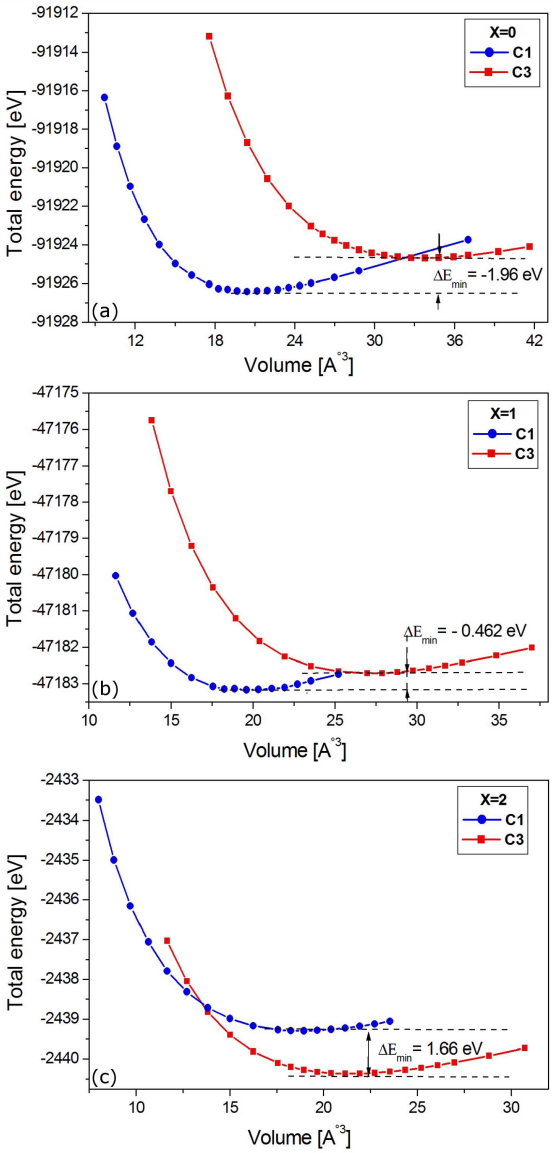

Fig. 2. Total energy versus volume for different structures of $Cu_xLi_{2-x}O$ ($x = 0$, 1, 2) system.

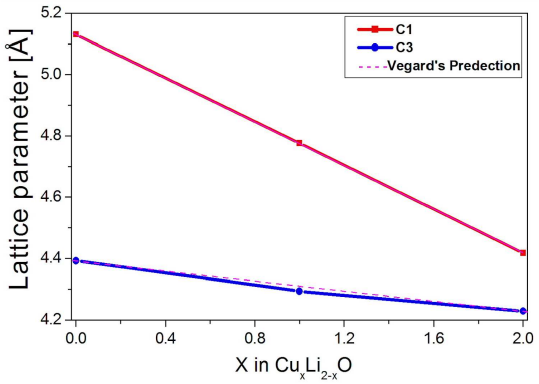

Fig. 3. Composition dependence of the calculated lattice constants (solid squares and circles) of $Cu_xLi_{2-x}O$ ($x = 0$, 1, 2) system compared with Vegard's prediction (magenta dashed line).

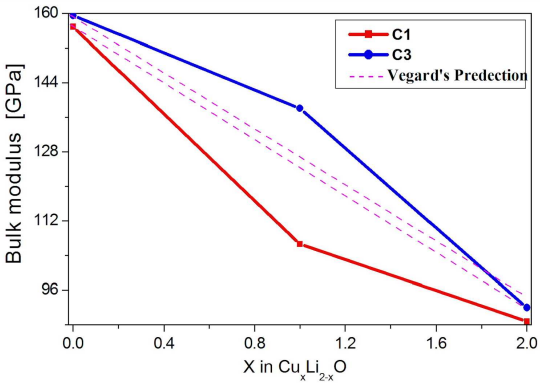

Fig. 4. Composition dependence of the calculated B (solid squares and circles) of $Cu_xLi_{2-x}O$ system compared with the linear composition dependence prediction (magenta dashed line).

where a_{AC} and a_{AB} are the equilibrium lattice constants of the binary compounds AC and AB, respectively, and $a(AB_{1-x}C_x)$ is the alloy lattice constant. Vegard's law (1) assumes that the alloy's lattice constant varies linearly with the composition. Deviation, however, usually occurs in semiconductor alloys, as was observed both experimentally and theoretically. Therefore, the alloy's lattice constant should be rewritten as

$$a\left(AB_{1-x}C_x\right) = xa_{AC} + (1-x)a_{AB} - x(1-x)b. \tag{2}$$

Here, in the quadratic term, b is the bowing parameter.

As shown in Fig. 3, the lattice constant decreases with increasing Cu composition (x). This is due to the fact that the Cu atom is smaller than the Li atom. Figure 3 shows that the calculated lattice constants for different alloy concentrations of the C_1 and C_3 structures obey Vegard's law with a slight upward bowing parameter of the value -0.002 Å and $+0.01$ Å, respectively. This indicates that the deviation from Vegard's law is much more pronounced for the C_3 structure. The bowing parameters were obtained by fitting the calculated values of a with the following polynomials of second order, namely:

$$a(x)_{C_1} = 5.13 - 0.35x + 0.002x^2, \tag{3}$$

$$a(x)_{C_3} = 4.375 - 0.0.09x + 0.0083x^2. \tag{4}$$

In Fig. 4, the bulk modulus as a function of composition x is presented. The decreasing behavior of B with the increase of Cu concentration (from $x = 0$ to $x = 2$) indicates, on the other hand, that the alloys become more compressible then. To obtain the bulk modulus fits, the following polynomials of second order were used:

$$B(x)_{C_1} = 159.54 - 9.15x - 12.32x^2, \tag{5}$$

$$B(x)_{C_3} = 188.56 - 52.68x + 2.182x^2. \tag{6}$$

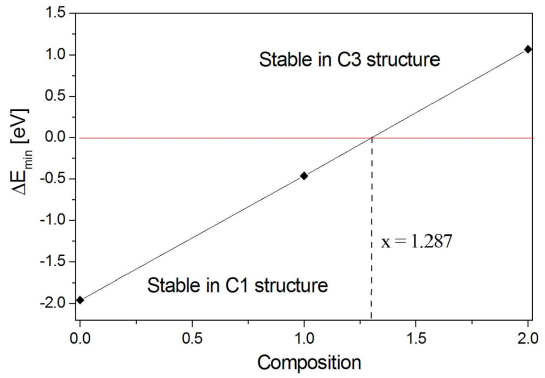

Fig. 5. Composition dependence of difference of lowest energy of $Cu_xLi_{2-x}O$ (x = 0, 1, 2) in C_1 and C_3 phases.

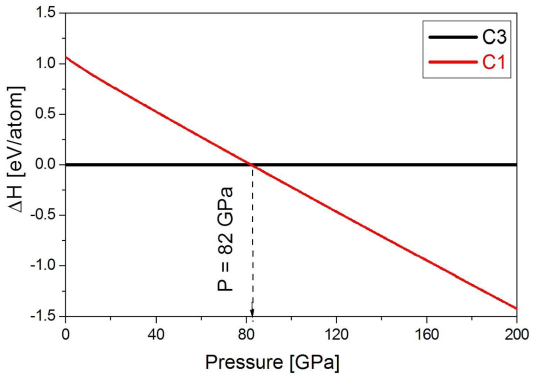

Fig. 6. Variation of the enthalpy differences ΔH as a function of pressure for Cu_2O in C_1 phase, the reference enthalpy in set for C_3 phase.

There is a small deviation from the linear concentration dependence with an upward bowing parameter of −12.32 GPa in the C_1 structure and downward bowing parameter of +16.26 GPa in the C_3 structure.

For materials with cubic structure, the melting point T_m (in K) correlates with the bulk modulus B (in GPa) by the following linear expression [31, 32]:

$$T_m = 607 + 9.3B. \quad (7)$$

Now, we could introduce the values of the bulk modulus into (7) in order to calculate the melting point T_m of the $Cu_xLi_{2-x}O$ (x = 0, 1, 2) system. For the antifluorite C_1 phase, the values obtained were found at around 2066, 1598, and 1432 K, for x = 0, 1 and 2, respectively. For the cuprite C_3 phase, the values obtained were found at around 2091, 1891, and 1462 K, for x = 0, 1 and 2, respectively. The melting temperature T_m = 1462 K of the cuprite C_3 phase of Cu_2O is in reasonable agreement with the experimental result equal to 1508 K (1235 °C) [21]. The deviation between these two values is around 3%.

Figure 5 shows a linear variation of the difference of the lowest energy between the antifluorite-type (C_1) and the cuprite-type (C_3) phase of the two structures, versus composition x. It is clearly seen that the $Cu_xLi_{2-x}O$ ternary alloy changes its most stable crystal structure from the C_1 to the C_3 phase when x is larger or equal to 1.287.

3.2. Phase transition

It is well known that high pressures influence the crystal packing of solid and its electronic structure. Thus, pressure plays an important role, affecting the materials properties in a super-conducting phenomenon, the elastic and thermal properties and structural phase transition [33, 34]. In order to get more information about the pressure-induced phase transition of crystals, we have to calculate the Gibbs free energies G of different considered phases. The following expression can be used [35, 36]:

$$G = E + PV - TS. \quad (8)$$

Here E, P, V, T, and S symbolize the total internal energy, pressure, volume, temperature, and entropy, respectively. Since our calculations were performed at T = 0 K, the last term TS becomes null, and consequently, the Gibbs free energy becomes equal to the enthalpy H, i.e., $H = E + PV$. For the Cu_2O material, the transition pressure (P_t) between the C_3 configuration and the C_1 phase was calculated using the enthalpy difference ΔH as a function of the pressure. The results were plotted in Fig. 6 with respect to the C_3 structure. This mentioned method, installed in the Mindlab program, has given excellent results [37–40].

Note that the transition from the C_3 phase to the C_1 phase may occur at the pressure value of 82 GPa, as shown in Fig. 6. At this pressure, the enthalpies of both structures become equal, while the enthalpy differences become null. To the best of our knowledge, there are no other data existing in the literature on the pressure-induced phase transition for Cu_2O. Our findings regarding the pressure phase transition of Cu_2O may be used as a reference for future works.

4. Conclusion

In this work, we have investigated the equilibrium structural parameters of Li_2O, Cu_2O and their alloy CuLiO in the antifluorite-type (C_1) and the cuprite-type (C_3) configurations. For this, we used the ab initio FP–LMTO method, within the LDA approximation. In general, our results agreed well with other data available in the literature, indicating that the used theoretical approach is reliable for the prediction of structural properties of the considered materials.

The results of the present studies concerned with the possibility of phase transition at high pressure show that Cu_2O material transforms from C_3 to C_1 at the pressure of around 82 GPa.

We have also found that the CuLiO alloy can change its most stable crystal structure from the antifluorite-type (C_1) to the cuprite-type (C_3) phase at the concentration value of x = 1.287.

References

[1] K. Kunc, I. Loa, *Phys. Status Solidi B* **9**, 242 (2005).

[2] E. Zintl, A. Harder, B. Dauth, *Z. Elektrochem.* **40**, 588 (1934).

[3] R.D. Eithiraj, G. Jaiganesh, G. Kalpana, M. Rajagopalan, *Phys. Status Solidi B* **244**, 1337 (2007).

[4] Hao Gao, Jian Sun, C.J. Pickard, R.J. Needs, *Phys. Rev. Mater.* **3**, 015002 (2019).

[5] J. Ghijsen, L.H. Tjeng, J.V. Elp, H. Eskes, J. Westerink, G.A. Sawatzky, M.T. Czyzyk, *Phys. Rev. B* **38**, 11322 (1988).

[6] V. Abhinav, V. Krishna Rao, P.S. Karthik, S.P. Singh, *RSC Adv.* **5**, 63985.

[7] N.S. Kim, S.Y. Hwang, E.Y. Kim, K.N. Han, *Jpn. J. Appl. Phys.* **49**, 05EA04 (2010).

[8] T.P. Yadav, G.C. Kaphle, A. Srivastava, *J. Nepal Phys. Soc.* **6**, 2934 (2020).

[9] S.Y. Savrasov, D.Y. Savrasov, *Phys. Rev. B* **46**, 12181 (1992).

[10] W. Kohn, L.J. Sham, *Phys. Rev.* **140**, A1133 (1965).

[11] L.J. Sham, W. Kohn, *Phys. Rev.* **145**, 561 (1966).

[12] Material Information and Design Laboratory, Department of Physics, University of California, Davis (CA).

[13] S.Y. Savrasov, arXiv:cond-mat/0409705, 2004.

[14] J.P. Perdew, Y. Wang, *Phys. Rev. A* **45**, 13244 (1992).

[15] X-P. Wei, T-Y. Cao, P. Gao, X-W. Sun, *Acta Phys. Pol. A* **138**, 440 (2020).

[16] J. Wu, J. Li, Y. Yu, Y. Yu, *CIESC J.* **71**, 192 (2020).

[17] A. Adjadj, H. Bouafia, B. Sahli, B. Djebour, S. Hiadsi, M. Ameri, *Acta Phys. Pol. A* **137**, 1101 (2020).

[18] H. Rekab-Djabri, M. Drief, M.M. Abdus Salam, S. Daoud, F. El Haj Hassan, S. Louhibi-Fasla, *Can. J. Phys.* **98**, 834 (2020).

[19] S. Hull, T.W.D. Farley, W. Hayes, M.T. Hutchings, *J. Nucl. Mater.* **160**, 125 (1988).

[20] Constitution of Binary Alloys, Ed. F.A. Shunk, 2nd Suppl., McGraw-Hill, New York 1969.

[21] B.K. Meyer et al., *The Physics of Copper Oxide (Cu_2O) in Semiconductors and Semimetals*, Vol. 88, Elsevier, 2013, Ch. 6, p. 201.

[22] M.M. Beg, S.M. Shapiro, *Phys. Rev. B* **13**, 1728 (1976).

[23] J. Hallberg, R.C. Hanson, *Phys. Status Solidi B* **42**, 305 (1970).

[24] P. Goel, N. Choudhury, S.L. Chaplot, *Phys. Rev. B* **70**, 174307 (2004).

[25] R. Dovesi, C. Roetti, C. Freyria-Fava, M. Prencipe, *Chem. Phys.* **156**, 11 (1991).

[26] A. Shukla, M. Dolg, P. Fulde, H. Stoll, *J. Chem. Phys.* **108**, 8521 (1998).

[27] A. Martínez-Ruiz, M.G. Moreno, N. Takeuchi, *Solid State Sci.* **5**, 291 (2003).

[28] E. Ruiz, S. Alvarez, P. Alemany, R.A. Evarestov, *Phys. Rev. B* **56**, 7189 (1997).

[29] P.A. Korzhavyi, B. Johansson, *Literature review on the properties of cuprous oxide Cu_2O and the process of copper oxidation*, Technical Report TR-11-08, 2011).

[30] L. Vegard, *Z. Phys.* **5**, 393 (1921).

[31] S. Daoud, P.K. Saini, H. Rekab-Djabri, *J. Nano-Electron. Phys.* **12**, 06008 (2020).

[32] M.E. Fine, L.D. Brown, H.L. Marcus, *Scr. Mater.* **18**, 951 (1984).

[33] P. Zhou, H.R. Gong, *J. Mech. Behav. Biomed. Mater.* **8**, 154 (2012).

[34] X.-W. Sun, N. Bioud, Z.-J. Fu, X.-P. Wei, T. Song, Z.-W. Li, *Phys. Lett. A* **380**, 3672 (2016).

[35] S. Zerroug, F. Ali Sahraoui, N. Bouarissa, *Appl. Phys. A* **97**, 345 (2009).

[36] Y.O. Ciftci, E. Ateser, *J. Electron. Mater.* **49**, 2086 (2020).

[37] H. Rekab-Djabri, M.M. Abdus Salam, S. Daoud, M. Drief, Y. Guermit, S. Louhibi-Fasla, *J. Magn. Alloy* **8**, 1166 (2020).

[38] H. Rekab-Djabri, S. Louhibi-Fasla, S. Amari, S. Bahlouli, M. Elchikh, *Eur. Phys. J. Plus* **132**, 471 (2017).

[39] R. Yagoub, H. Rekab-Djabri, S. Daoud, S. Louhibi-Fasla, M.M. Abdus Salam, S. Bahlouli, M. Ghezali, *Comput. Condens. Matter.* **23**, e00452 (2020).

[40] H. Rekab-Djabri, R. Khatir, S. Louhibi-Fasla, I. Messaoudi, H. Achour, *Comput. Condens. Matter.* **10**, 15 (2017).